A method to measure specific absorption rate of nanoparticles in colloidal suspension using different configurations of radio-frequency fields

Dhivya Ketharnath,[1,2] Rohit Pande,[1,2] Leiming Xie,[1] Srimeenakshi Srinivasan,[3] Biana Godin,[3] and Jarek Wosik[1,2]

[1]Electrical and Computer Engineering Department, University of Houston, Houston, Texas 77204, USA
[2]Texas Center for Superconductivity, University of Houston, Houston, Texas 772042, USA
[3]Department of Nanomedicine, The Methodist Hospital Research Institute, Houston, Texas, 77030, USA

We report a method for characterization of the efficiency of radio-frequency (*rf*) heating of nanoparticles (NPs) suspended in an aqueous medium. Measurements were carried out for water suspended 5 nm superparamagnetic iron-oxide NPs with 30 nm dextran matrix for three different configurations of *rf* electric and magnetic fields. A 30 MHz high-Q resonator was designed to measure samples placed inside a parallel plate capacitor and solenoid coil with or without an *rf* electric field shield. All components of *rf* losses were analyzed and *rf* electric and magnetic field induced heating of NPs and the dispersion medium was determined and discussed. © 2012 American Institute of Physics. [http://dx.doi.org/10.1063/1.4748285]

Currently employed *rf* hyperthermia and ablation techniques, even if minimally invasive, are non-selective and frequently induce thermal necrosis even to normal cells surrounding *rf* ablation probes.[1] It has been demonstrated that *rf* procedures can be non-invasive and cell-selective when an external *rf* source is used in conjunction with either directly or systemically injected functionalized nanoparticles (NPs), acting as *rf* absorption enhancers.[2–4]

To quantify *rf* heat enhancement due to the presence of NPs in colloidal aqueous or physiological suspensions, their specific absorption rate (SAR) as a dosimetric parameter has to be determined.[5] Heating related properties of magnetic NPs were studied for many years, which resulted in significant progress in employing magnetic particles in research and in clinical applications.[4,6,7] The un-normalized SAR values for such magnetic nanoparticles for different field strengths and frequencies were reported by several research groups to be in a range from 15 to 4000 W/g.[3,7–14] Also, for non-magnetic NPs, such as single-walled carbon nanotubes, and gold NPs, a significant *in-situ* heating as well as *in-vitro* heat destruction of malignant cells have been found.[15–19]

The *rf* loss for single-domain ferromagnetic or superparamagnetic nanoparticles (SPNPs) suspended in a colloidal fluid is described by two parallel relaxation processes, Brownian and Néel.[9,11] In Brownian relaxation, the NP physically rotates to align with the field while in Néel relaxation, the magnetic moment rotates internally within the NP. In smaller NPs, the loss is dominated by Neel relaxation while in larger NPs Brownian relaxation is the prevailing mechanism.[20]

While the *rf* heating of colloidal suspensions as a whole is well documented,[4,8,21,22] the contribution of dispersion medium's or solution's heating to overall heating of the NP suspension has generally been overlooked.[23] At low frequencies (kHz), the contribution of the solution to the overall heat loss is relatively small and can be neglected. However, this assumption is invalid at higher frequencies (MHz), where the conducting behavior of the solution is dominant and hence has a significant influence on the measured heating.

In order to determine SAR of SPNPs, usually the temperature change of a NPs suspension is measured using a long closely wound solenoid coil. Such solenoid produces a time-varying uniform *rf* magnetic field H_z in the axial z-direction. From Faraday's law of induction, H_z produces a time-varying electric field referred to as magnetically induced electric field E_ϕ, oriented in the circumferential ϕ-direction. Additionally, there exists an axial electric field E_z caused by the scalar electric potential due to the coil winding, where ρ, ϕ, z are the cylindrical coordinates.[24] So far, for SAR measurements, only E_ϕ has been considered responsible for eddy currents losses and H_z for spin related losses, but the existence of the conservative electric field E_z was, surprisingly, disregarded.[10,13] However, the magnitude of the E_z component in most solenoid configurations is at least comparable to the magnitude of the E_ϕ component and significantly contributes to the total *rf* electric field $E_s = E_\phi + E_z$ and can thus affect the sample heating.[25] Neglecting the heating due to interaction of the E_z with both NPs and their solution may lead to overestimation of the *rf* magnetic field related SAR of the NPs.

In this paper, we have experimentally and numerically analyzed the *rf* losses due to interaction of both NPs and the solution with electric (E_{rf}) and magnetic (H_{rf}) fields. This method can generally be applied to any type of NP; however, this paper focuses on measurements of superparamagnetic iron oxide (SPIO) NPs. We will demonstrate how the combination of both *rf* fields allows for determination of three heating components, which are related to NP *rf* electric field, NP *rf* magnetic field, and the solution only losses.

Our experimental setup is based on a high Q inductance-capacitance-resistance (LCR) resonator, which can generate high E_{rf} and H_{rf} fields up to 100 kV/m and 50 kA/m respectively, in the 12–50 MHz frequency range at low input power. A block diagram of the experimental set up is shown in Fig. 1. The resonator's capacitor is constructed with two copper plates separated by 12 mm thick single crystal sapphire block ($\varepsilon_r = 11$, $\tan \delta = 10^{-5}$). The resonator's solenoid
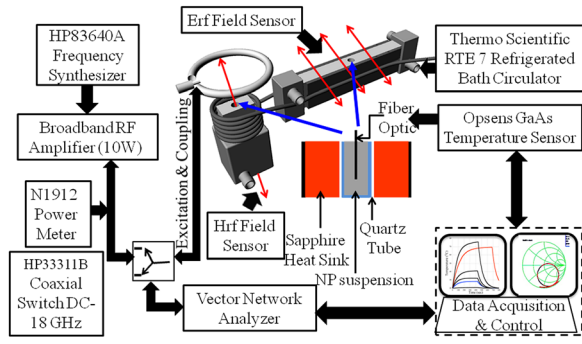
FIG. 1. *Rf* heating measurement set-up with water-cooled LCR resonator consisting of a parallel plate capacitor and solenoid.

is made of six turns of copper tube wound into a coil of diameter 40 mm and distance per turn of 0.1 mm. The design of the resonator enables the sample to be held in a quartz tube positioned in cylindrical cavities drilled in the capacitor's and solenoid's sapphire blocks. The sapphire crystals, copper plates, and windings are water-cooled by a refrigerated bath circulator (Thermo Scientific) to maintain a constant sink temperature of 20 °C. An HP 83640 A frequency synthesizer and 10 W (1–500 MHz) *rf* amplifier are used to drive the resonator *via* an inductive coupling loop. The field components in the resonator are measured using an electric dipole and a loop sensor. Temperature is recorded versus time by GaAs (Opsens) sensor controlled by a micro-meter modulated stage translation.

Using the finite element method (FEM) simulator tool Ansoft HFSS, we performed simulations of field components in the solenoid and the capacitor. To study the individual effects of the E_z and E_ϕ fields in the solenoid, we vary the E_z since E_ϕ cannot be altered without affecting the *rf* source. Hence, the effect of E_ϕ on the sample was analyzed while suppressing E_z by imposing a perfect-electric-conductor (PEC) boundary condition, where the electric field is normal while the magnetic field is tangential to the surface. This boundary condition is incorporated by using a cylindrical copper shield with longitudinal either single or multi gaps (to prevent eddy currents) inserted in the solenoid.

Rf fields in the solenoid for samples with different permittivity and conductivity were simulated. Fig. 2 shows results for three cases: (a) an empty (filled with air) quartz tube ($\varepsilon_r = 1$, $\sigma = 0$ S/m), (b) quartz tube filled with physiological saline solution ($\varepsilon_r = 81$, $\sigma = 1$ S/m), and (c) air (empty tube) with shield. The simulated effect of the copper shield on the E_ϕ, E_z, and H_z field components in the solenoid clearly demonstrate strong suppression of the E_z with only slight reduction of the E_ϕ and H_z components.

For the experimental SAR measurements using our approach, we investigated heating of water suspended SPIO NPs (Sienna + ®) from Endomagnetics Ltd. The SPIO NPs were characterized for average diameter, size distribution, and zeta potential using ZetaSizer Nano ZS (Malvern). The measurement of the average diameter of dextran surrounding 5 nm iron-oxide cores was found to be ∼31.7 nm. The zeta potential measurements show that the particles have a negative zeta potential (−24.6 mV) which allows them to be in a monodispersed colloidal form.
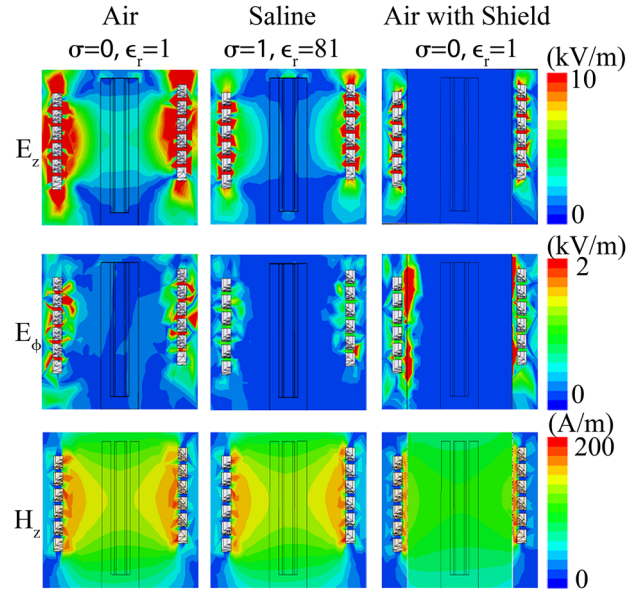

FIG. 2. Magnitude of conservative electric field E_z, magnetically induced electric field E_ϕ, and magnetic field H_z are shown for solenoid with quartz tube containing air sample (left images); conducting sample (central images) and air sample with copper shield (right images).

Three different *rf* field configurations, shown in Fig. 3 have been used for measurements of the temperature T as a function of time t for 150 µl SPIO samples for an input of 1 W. Three slopes ($q = dT/dt$) q^c, q^{s0}, and q^{ss} were measured for the capacitor (E_y), the solenoid (E_ϕ, E_z, and H_z), and the shielded solenoid (E_ϕ and H_z), respectively, from initial 20 s of the initial slopes as shown in Fig. 4.

Heat loss per unit volume of the sample P (W/m^3) can be expressed in terms of E_{rf} and H_{rf} components as

$$P = C_{ps}\rho_s q^m = \frac{1}{2}\left(\sigma_{sus}[\gamma^m(\sigma_{sol})|E_L^m|^2] + \mu_0\omega\chi''|H_z^m|^2 v_f\right).$$

(1)

Here, C_{ps} is the constant pressure specific heat (J/(kgK)), ρ_s is the mass density (kg/m^3), q is the slope dT/dt, σ represents electric conductivity of the sample, $\gamma(\sigma)$ is the depolarization factor due to the free ion charges in the sample, v_f is the volume fraction of SPIO NPs in the suspension, E_L is the local electric field in the sample region, and ω is the resonant frequency. SAR (P/ρ_s) can also be calorimetrically expressed as $C_{ps}dT/dt$ (W/kg). The specific heat capacity and density of the solution are used as those of water. The superscript *m*
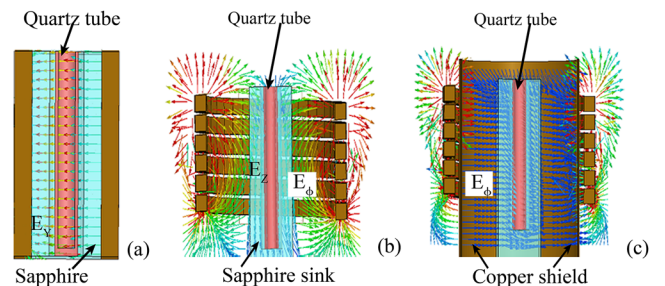

FIG. 3. E_{rf} and H_{rf} vector components distribution in (a) parallel plate capacitor (E_y), (b) solenoid ($E_s = E_\phi + E_z$), and (c) solenoid with gapped copper shield (H_z and E_ϕ).
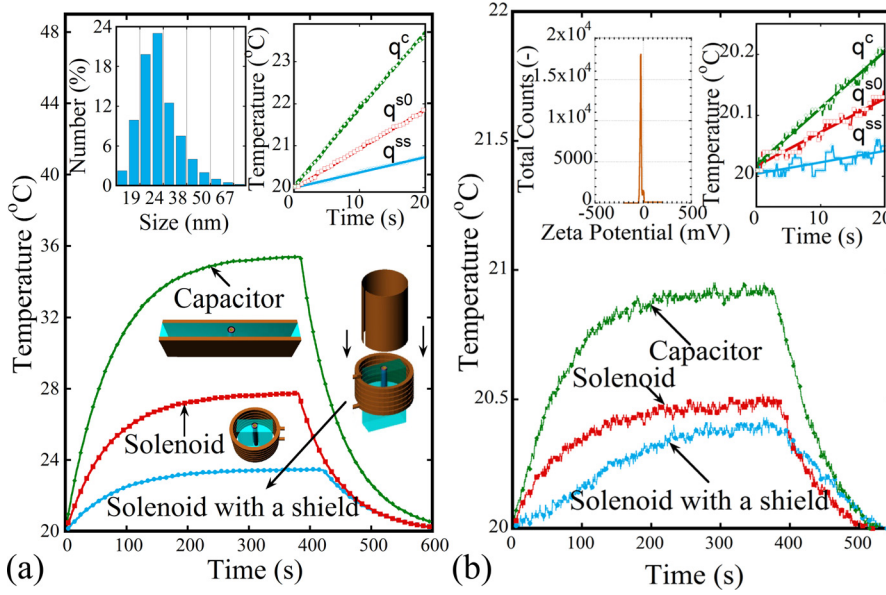
FIG. 4. Temperature dependence on time plotted for (a) 28 mg/ml, (b) 1 mg/ml SPIO suspension samples measured in three *rf* fields configurations. Insets show q^m slopes and linear dependence of T on t during first 20 s of heating. The other two insets depict NPs overall size and zeta potential distribution.

refers to the three cases of the sample being placed in the capacitor *c*, solenoid *s0*, and/or solenoid with shield *ss*. Hence, in solenoid $E_L^{s0} = E_s$, in solenoid with the shield $E_L^{ss} = E_\phi$ and in the capacitor $E_L^c = \beta E_y$, where β is the dielectric polarization screening factor. The depolarization factor $\gamma^m(\sigma)$ for the solenoid with and without shield are $\gamma^{ss}(\sigma) \equiv 1$ and $\gamma^{ss0}(\sigma) \cong 1$, respectively. For the capacitor, it can be expressed as a Debye factor since the sample is perpendicular to E_L

$$\gamma(\sigma) = \left| \frac{1}{1 + j\left(\frac{\omega_p(\sigma)}{\omega}\right)} \right|^2 = \frac{1}{1 + \left(\frac{\omega_p(\sigma)}{\omega}\right)^2}. \tag{2}$$

Here, $\omega_p(\sigma) = \sigma L/\pi a \varepsilon_0 \varepsilon_s$, with sample tube length L = 15 mm and inner radius a = 1.4 mm. $\varepsilon_0 \varepsilon_s$ is the permittivity of the NP solution.

In order to determine the exact value of the electric and magnetic field components in the solenoid and capacitor, a solution of known conductivity is measured. In our system, for calibration of the LCR resonator 2.5 mM NaCl salt solution ($\sigma_{salt} = 0.0314$ S/m, $\gamma^c = 0.57$, $\chi'' = 0$, $v_f = 0$) was used as a reference. Respective slopes were used to determine the local electric field components (in solenoid $E_L^{s0} = E_s$, in solenoid with the shield $E_L^{ss} = E_\phi$ and in the capacitor $E_L^c = \beta E_y$) from Eq. (1) and their values are given in Table I. When the screening factor $\beta = 0.11$ obtained from simulations using HFSS, and the E_L values shown in the Table I were used to calculate the applied field E_y across the capacitor, we obtained 31.4 kV/m. This value is very close to the voltage

sensor measured value. The conservative electric field component $E_z = \sqrt{(E_s)^2 - (E_\phi)^2}$ is estimated as 1.7 kV/m.

The two concentrations of SPIO NPs 28 mg/ml and 1 mg/ml studied here had volume fractions $\nu_{f1} = 5.4 \times 10^{-3}$ and $\nu_{f2} = 1.96 \times 10^{-4}$. The heating slopes for the different configurations are summarized in Table II. Since there is no magnetic loss involved in the capacitor ($H_{rf} = 0$), from Eq. (1) substituting q^c for the two samples, we have calculated the conductivity of the suspensions as $\sigma_{sus1} = 0.13$ S/m and $\sigma_{sus2} = 0.0065$ S/m. Further, for a colloidal suspension, the effective conductivity of the NPs suspension in the capacitor can be expressed as

$$\sigma_{sus} = \sigma_{NP}\nu_f + \sigma_{sol}(1 - \nu_f). \tag{3}$$

Substituting both the volume fractions ν_{f1} and ν_{f2} and calculated effective conductivities σ_{sus1} and σ_{sus2} of the two samples in Eq. (3), the unknown variables σ_{NP} and σ_{sol} were solved and the conductivities of the SPIO-dextran NP complex and the dispersion medium were estimated as $\sigma_{NP} = 23.3$ S/m and $\sigma_{sol} = 0.002$ S/m.

In order to determine the magnetic loss of the SPIO NPs, the calorimetric equations for the sample in the solenoid with shield were obtained from Eq. (1),

$$C_{ps}\rho_s q_{sus}^{ss} = \frac{1}{2}\left(\sigma_{sus}|E_\varphi|^2 + \mu_0\omega\chi''|H_z|^2 v_f\right) \tag{4}$$

from which susceptibility can be extracted as

$$\chi'' = \left(\frac{2C_{ps}\rho_s q_{sus}^{ss} - \sigma_{sus}|E_\phi|^2}{\mu_0\omega|H_z|^2 v_f}\right). \tag{5}$$

TABLE I. Slope (q = dT/dt) values of NaCl and calculated local fields values for the three configurations.

Configuration	Slope q$_{salt}$	Local electric field E$_L$ (kV/m)	H$_z$ (kA/m)
Capacitor "c"	0.02557	3.46 (βE_y)	0
Solenoid "s0"	0.01408	1.936 (E_s)	8.2
Solenoid with shield "ss"	0.00227	0.776 (E_ϕ)	7.1

TABLE II. Slope values (q = dT/dt) of SPIO for the three configurations.

Configuration	Slope q_{spio}^m (28 mg/ml)	Slope q_{spio}^m (1 mg/ml)
Capacitor "c"	0.1832	0.009255
Solenoid "s0"	0.093635	0.005501
Solenoid with shield "ss"	0.0364	0.001868

TABLE III. SAR values for respective SPIO concentrations. ($H_z = 7.1$ kA/m, $E_s = 1.91$ kV/m, f = 30 MHz).

Concentration (mg/ml)	χ''	SAR$_M$ (kW/kg)	SAR$_M$/fH^2 (Wsm^2/kgA^2)	SAR$_E$ (kW/kg)	SAR$_E$/fE^2 (Wsm^2/kgV^2)
28	0.0038	4.1	2.9×10^{-12}	8.5	8.1×10^{-11}
1	0.0055	5.86	4.2×10^{-12}	8.5	8.1×10^{-11}

Substituting fields and slopes from Tables I and II, we get $\chi''_1 = 0.0038$ for 28 mg/ml SPIO and $\chi''_2 = 0.0055$ for 1 mg/ml SPIO NP suspensions. The magnetic component of SAR (SAR$_M$) of the SPIO NPs can be expressed as follows:

$$SAR_M = \frac{\mu_0 \chi''}{2\rho_{NP}} \omega |H_z|^2. \quad (6)$$

For magnetic and non-magnetic NPs *rf* power loss is proportional to $\omega H^2 \chi''(f)$ and $\sigma(\omega)E^2$, respectively. For the frequency range $10^5 - 10^6$ Hz, χ'' and σ has no frequency dependence.[24] Originally SAR was introduced as a parameter describing a dose of energy absorbed by a body due to *rf* electromagnetic wave irradiation.[26] Later it was adopted to describe the *rf* loss enhancement due to NPs. However for such a case, in order to describe the intrinsic *rf* loss of NPs, SAR has to be normalized by frequency and by the square of the magnetic or electric field. Only this normalization allows for comparison of SAR measured at different frequencies and at different *rf* fields.

At a particular electric field, *rf* electric field induced SAR can be calculated from the power loss P as

$$SAR_E = \frac{\sigma_{sample}}{2\rho_{sample}} |E_s|^2. \quad (7)$$

From the mass density of the SPIO $\rho_{NP} = 5.17 \times 10^3$ kg/m^3 and that of the solution $\rho_{sol} = \rho_{water} = 10^3$ kg/m^3, we calculated SAR of the NPs and solution for electric field $E_s = 1.91$ kV/m as 8.5 kW/kg and 3.8 W/kg, respectively. The normalized value of the NP SAR$_E$ is equal to 8.1×10^{-11} Wsm^2/kgV^2 and it is the same for both our samples. The values of SAR$_E$ and SAR$_M$ at frequency 30 MHz and the magnetic field strength 7.1 kA/m are given in Table III.

The origin of this loss cannot be explained by ohmic and/or dielectric loss of the dextran matrix and the most plausible cause is the NP-dextran-solution interface loss.[27] Since NPs are charged, ionic double-layers are formed around the particles acting as additional source of E_{rf} induced loss. Surface polarization of the NP due to E_{rf} will enhance this interaction accounting for heat loss leading to such SAR$_E$ value.

The elucidation of the mechanisms of NPs heating in electric/magnetic fields is very important for designing therapeutic systems for targeted hyperthermia. Unlike the processes involved in NPs' heating in the kHz range, clinically used cancer hyperthermia devices are based on the frequencies in the MHz range.[28] At these higher frequencies, the contribution of the dispersion medium to the overall heat loss cannot be neglected. The method introduced here allows us to distinguish and to calculate specifically the contributions of the E_{rf} and H_{rf} to the overall heating efficiency. It can be calculated from Eq. (1) that if the electric field ($E_s = E_L^{s0}$) induced loss is neglected, as it is done in litera-

ture, all heat produced by E field will be counted as magnetic loss, and the magnetic SAR$_M$ for sample 1 will be 14 kW/kg ($\chi'' = 0.013$). This is a very significant difference compared to the more accurate value of 4.1 kW/kg ($\chi'' = 0.0038$) obtained in this paper (giving 250% systematic error).

[1]J. van der Zee, Ann. Oncol. **13**(8), 1173 (2002).
[2]M. Kallumadil, M. Tada, T. Nakagawa, M. Abe, P. Southern, and Q. A. Pankhurst, J. Magn. Magn. Mater. **321**(10), 1509 (2009).
[3]Q. A. Pankhurst, J. Connolly, S. K. Jones, and J. Dobson, J. Phys. D: Appl. Phys. **36**(13), R167 (2003).
[4]P. Wust, U. Gneveckow, M. Johannsen, D. Böhmer, T. Henkel, F. Kahmann, J. Sehouli, R. Felix, J. Ricke, and A. Jordan, Int. J. Hyperthermia **22**(8), 673 (2006).
[5]T. Z. Wong, J. W. Strohbehn, K. M. Jones, J. A. Mechling, and B. S. Trembly, IEEE Trans. Microwave Theory Tech. **34**(5), 560 (1986).
[6]A. Jordan, P. Wust, H. Föhling, W. John, A. Hinz, and R. Felix, Int. J. Hyperthermia **25**(7), 499 (2009).
[7]B. Thiesen and A. Jordan, Int. J. Hyperthermia **24**(6), 467 (2008).
[8]E. Kita, S. Hashimoto, T. Kayano, M. Minagawa, H. Yanagihara, M. Kishimoto, K. Yamada, T. Oda, N. Ohkohchi, T. Takagi, T. Kanamori, Y. Ikehata, and I. Nagano, J. Appl. Phys. **107**(9), 09B321 (2010).
[9]S. Laurent, S. Dutz, U. O. Hofeli, and M. Mahmoudi, Adv. Colloid Interface Sci. **166**(1-2), 8 (2011).
[10]M. Ma, Y. Wu, J. Zhou, Y. Sun, Y. Zhang, and N. Gu, J. Magn. Magn. Mater. **268**(1-2), 33 (2004).
[11]S. Purushotham and R. V. Ramanujan, J. Appl. Phys. **107**(11), 114701 (2010).
[12]J. H. Lee, J. Jang, J. Choi, S. H. Moon, S. Noh, J. Kim, J. G. Kim, I. S. Kim, K. I. Park, and J. Cheon, Nat. Nanotechnol. **6**(7), 418 (2011).
[13]Y. Yuan and D. Tasciuc, J. Magn. Magn. Mater. **323**(20), 2463 (2011).
[14]R. Hergt and S. Dutz, J. Magn. Magn. Mater. **311**(1), 187 (2007).
[15]D. E. Kruse, D. N. Stephens, H. A. Lindfors, E. S. Ingham, E. E. Paoli, and K. W. Ferrara, IEEE Trans. Biomed. Eng. **58**(7), 2002 (2011).
[16]C. J. Gannon, P. Cherukuri, B. I. Yakobson, L. Cognet, J. S. Kanzius, C. Kittrell, R. B. Weisman, M. Pasquali, H. K. Schmidt, R. E. Smalley, and S. A. Curley, Cancer **110**(12), 2654 (2007).
[17]E. S. Glazer, C. Zhu, K. L. Massey, C. S. Thompson, W. D. Kaluarachchi, A. N. Hamir, and S. A. Curley, Clin. Cancer Res. **16**(23), 5712 (2010).
[18]P. Cherukuri, E. S. Glazer, and S. A. Curley, Adv. Drug Delivery Rev. **62**(3), 339 (2010).
[19]C. Moran, S. Wainerdi, T. Cherukuri, C. Kittrell, B. Wiley, N. Nicholas, S. A. Curley, J. Kanzius, and P. Cherukuri, Nano Res. **2**(5), 400 (2009).
[20]R. E. Rosensweig, J. Magn. Magn. Mater. **252**, 370 (2002).
[21]X. Wang, H. Gu, and Z. Yang, J. Magn. Magn. Mater. **293**(1), 334 (2005).
[22]I. Baker, Q. Zeng, W. Li, and C. R. Sullivan, J. Appl. Phys. **99**(8), 08H106 (2006).
[23]S. Mornet, S. Vasseur, F. Grasset, and E. Duguet, J. Mater. Chem. **14**(14), 2161 (2004).
[24]F. S. Chute and F. E. Vermeulen, IEEE Trans. Edu. **24**(4), 278 (1981).
[25]B. Park, A. G. Webb, and C. M. Collins, J. Magn. Res. **199**(2), 233 (2009).
[26]B. J. Klauenberg and D. Miklavcic, *Radio Frequency Radiation Dosimetry and its Relationship to the Biological Effects of Elecromagnetic Fields* (Kluwer Academic, Dordrecht, 2000).
[27]J. Wosik, L. Xie, R. Pande, D. Ketharnath, Z. Chikani, S. Srinivasan, and B. Godin, "Mechanism of rf heating of metallic and dielectric nanoparticles" (unpublished).
[28]A. Y. Cheung and A. Neyzari, Cancer Res. **44**(10 Suppl.), 4736 (1984).